Author(s): Såmark-Roth, A.; Cox, D. M.; Rudolph, D.; Sarmiento, L. G.; Albertsson, M.; Carlsson, B. G.; Egido, J. L.; Golubev, P.; Heery, J.; Yakushev, A.; Åberg, S.; Albers, H. M.; Block, M.; Brand, H.; Calverley, T.; Cantemir, R.; Clark, R. M.; Düllmann, Ch. E.; Eberth, J.; Fahlander, C.; Forsberg, U.; Gates, J. M.; Giacoppo, F.; Götz, M.; Götz, S.; Herzberg, R.-D.; Hrabar, Y.; Jäger, E.; Judson, D.; Khuyagbaatar, J.;

Title: Spectroscopy along flerovium decay chains. III : Details on experiment, analysis, 282Cn, and spontaneous fission branches

Year: 2023

Version: Published version

Spectroscopy along flerovium decay chains. III. Details on experiment, analysis, ^{282}Cn, and spontaneous fission branches

A. Såmark-Roth,[1,*] D. M. Cox,[1] D. Rudolph,[1] L. G. Sarmiento,[1] M. Albertsson,[1] B. G. Carlsson,[1] J. L. Egido,[2] P. Golubev,[1] J. Heery,[3,†] A. Yakushev,[4,5] S. Åberg,[1] H. M. Albers,[4] M. Block,[4,5,6] H. Brand,[4] T. Calverley,[3] R. Cantemir,[4] R. M. Clark,[7] Ch. E. Düllmann,[4,5,6] J. Eberth,[8] C. Fahlander,[1] U. Forsberg,[7] J. M. Gates,[7] F. Giacoppo,[4,5] M. Götz,[4,5,6] S. Götz,[4,5,6] R.-D. Herzberg,[3] Y. Hrabar,[1] E. Jäger,[4] D. Judson,[3] J. Khuyagbaatar,[4,5] B. Kindler,[4] I. Kojouharov,[4] J. V. Kratz,[6] J. Krier,[4] N. Kurz,[4] L. Lens,[4,6,‡] J. Ljungberg,[1] B. Lommel,[4] J. Louko,[9] C.-C. Meyer,[5,6] A. Mistry,[10,4] C. Mokry,[5,6] P. Papadakis,[3,§] E. Parr,[4] J. L. Pore,[7] I. Ragnarsson,[1] J. Runke,[4,6] M. Schädel,[4] H. Schaffner,[4] B. Schausten,[4] D. A. Shaughnessy,[11] P. Thörle-Pospiech,[5,6] N. Trautmann,[6] and J. Uusitalo[9]

[1]*Department of Physics, Lund University, 22100 Lund, Sweden*
[2]*Departamento de Física Teórica and CIAFF, Universidad Autónoma de Madrid, 28049 Madrid, Spain*
[3]*Department of Physics, University of Liverpool, Liverpool L69 7ZE, United Kingdom*
[4]*GSI Helmholtzzentrum für Schwerionenforschung GmbH, 64291 Darmstadt, Germany*
[5]*Helmholtz Institute Mainz, 55099 Mainz, Germany*
[6]*Department Chemie-Standort TRIGA, Johannes Gutenberg-Universität Mainz, 55099 Mainz, Germany*
[7]*Nuclear Science Division, Lawrence Berkeley National Laboratory, Berkeley, California 94720, USA*
[8]*Institut für Kernphysik, Universität zu Köln, 50937 Köln, Germany*
[9]*Department of Physics, University of Jyväskylä, 40014 Jyväskylä, Finland*
[10]*Institut für Kernphysik, Technische Universität Darmstadt, 64289 Darmstadt, Germany*
[11]*Nuclear and Chemical Sciences Division, Lawrence Livermore National Laboratory, Livermore, California 94550, USA*

(Received 12 April 2022; revised 19 December 2022; accepted 4 January 2023; published 6 February 2023)

Flerovium isotopes (element $Z = 114$) were produced in the fusion-evaporation reactions ^{48}Ca + ^{242,244}Pu and studied with an upgraded TASISpec decay station placed in the focal plane of the gas-filled separator TASCA at the GSI Helmholtzzentrum für Schwerionenforschung in Darmstadt, Germany. Twenty-nine flerovium decay chains were identified by means of correlated implantation, α decay, and spontaneous fission events. Data analysis aspects and statistical assessments, primarily based on measured rates of various events, which laid the foundation for the comprehensive spectroscopic information on the flerovium decay chains, are presented in detail. Various decay scenarios of an excited state observed in ^{282}Cn are examined in depth with the help of GEANT4 simulations and assessed by predictions of beyond mean-field calculations including triaxial shape degrees of freedom. Previous, revised, and newly derived fission probabilities of even-even superheavy nuclei are compared with various theoretical predictions.

DOI: 10.1103/PhysRevC.107.024301

I. INTRODUCTION

Discovery of new superheavy elements [1–4] is being followed by sophisticated single-atom chemistry experiments [5–8] and nuclear spectroscopy experiments [9–12]. Such chemical and spectroscopic investigations have focused or relied on α-decay chains stemming from elements 114, Fl, or element 115, Mc. The practical reason is that isotopes of these elements are known to have the largest production cross sections in this region on the order of $\sigma \approx 5$–10 pb [2,12,13]. For decay spectroscopy studies conducted with instruments placed directly behind recoil separators, this corresponds to the observation of about one to two decay chains of superheavy atomic nuclei per day. The main incentive of such studies is to provide reliable experimental anchor points at the uppermost end of the nuclear chart for nuclear structure theory, which otherwise has to solely rely on extrapolations over many units of atomic (Z) and neutron (N) numbers [14]. The

*anton.samarkroth@gmail.com
†Present address: Department of Physics, University of Surrey, Guildford GU2 7XH, United Kingdom.
‡Present address: Institut für Physikalische Chemie und Radiochemie, Hochschule Mannheim, 68163 Mannheim, Germany.
§Present address: STFC Daresbury Laboratory, Daresbury, Warrington WA4 4AD, United Kingdom.

main goal is to gain access to decay schemes relevant for nuclear structure physics (see, e.g., Fig. 5 in Ref. [9]). Reliability in the interpretation of the measured spectra is being consolidated through self-consistency checks in GEANT4-based virtual experiments [15–17].

Another incentive to study flerovium isotopes in particular is that many microscopic-macroscopic nuclear structure models or model parametrizations suggest $Z = 114$ as the next magic proton number beyond lead, $Z = 82$, while modern mean-field approaches tend to favor $Z = 120$ [18,19]. Recent spectroscopic benchmarks on even-even flerovium isotopes, which are given in Ref. [20], demonstrate the need to consider various shape degrees of freedom [21] as well as correlations beyond the mean-field level [22]. An interesting facet of superheavy odd-A nuclei in experimental reach is the predicted presence and competition between high-j and low-j orbitals at low excitation energies [23–27]. Though details can differ widely among different theories, the common feature is that at least two α-decay sequences can be expected for a given isotope [12]. In connection with K-converted electromagnetic transitions, there are also opportunities for X-ray fingerprinting of the isotope's proton number [28].

Based on ^{48}Ca-induced fusion-evaporation reactions on Pu target material, the first decay chains associated with flerovium isotopes were put forward more than two decades ago [29,30]. While the isotopic origin of these early results remains ambiguous (see, for instance, notes in Refs. [13,31,32]), a more coherent picture of the generic decay characteristics of $^{284–289}$Fl emerged over time [2,32,33] from a number of discovery and confirmation experiments conducted at various accelerator facilities. These include both direct and indirect flerovium production [13,34–45]. However, the combined decay data for a given isotope is insufficient for detailed nuclear structure assessments; it lacks either an appropriate number of events, or spectroscopic relevance, or both. This is illustrated in the Supplemental Materials of Refs. [20,46].

In the present work, details of a spectroscopy experiment aiming to study decay chains originating from flerovium isotopes are described, complementing the results presented elsewhere on even-even ^{286,288}Fl [20] and odd-A ^{289}Fl [46]. Here, the focus is on analysis aspects and various statistical assessments of the underlying data set, guiding towards Tables I in the Supplemental Materials of Refs. [20,46] and the present article [47], respectively. These tables summarize the information on correlated α-decay chains, which were observed in the present study. The vast majority of the chains could be associated with decays of flerovium isotopes [20,46].

The experiment is described in Sec. II. Special emphasis is put on the isotopic composition of the different target segments on the target wheels, Fl-isotope assignment, and measured cross sections. Aspects of first-level data analysis are summarized in Sec. III. Coincidence events between α particles detected in the implantation double-sided silicon strip detector (DSSD) and electrons in the box DSSDs are described. Further details are provided in the Supplemental Material [47]. These concern:

(i) the method that was used to derive N_{random}, i.e., the number of apparent decay chains of a given type expected to arise randomly from background;
(ii) a likelihood assessment of missing events, and in particular missed implantation events;
(iii) the treatment of so-called escape events, i.e., when α-decay events leave merely a fraction of their decay energy only in the central DSSD;
(iv) the procedure used to determine α-decay energies;
(v) comments on germanium detector data processing and randomly correlated photon coincidences.

Section IV begins with a more comprehensive investigation of the internal decay of the state identified at ≈0.6 MeV excitation energy in ^{282}Cn [20]. Four decay scenarios are investigated with GEANT4 simulations and assessed with the help of transition strengths predicted with beyond mean-field calculations, which include triaxial shapes [22]. Decay probabilities for α- and spontaneous-fission branches for a number of even-even superheavy nuclei are compiled and discussed in Sec. IV B. The paper closes with a summary in Sec. V.

II. EXPERIMENT

The experiment was conducted at the GSI Helmholtzzentrum für Schwerionenforschung, Darmstadt, Germany, in two runs in 2019 and 2020. Table I summarizes the main parameters. A $^{48}Ca^{10+}$ beam was accelerated with the Universal

TABLE I. Summary of experimental parameters: ^{242}Pu and ^{244}Pu target segments, Ti backing and degrader thicknesses, midtarget beam energies and compound-nucleus excitation energies, measured beam integrals, and number of decay chains associated with the $4n$ channel, ^{286,288}Fl, as well as the $3n$ channel ^{287,289}Fl for the two experimental runs 1 and 2. Derived cross sections, $\sigma(4n)$ and $\sigma(3n)$, are given as well, likewise the value corresponding to the observation of one Fl-decay chain in the last row. See text for further details.

Target	^{242}Pu		^{244}Pu	
Pu layer (mg/cm^2)	0.71(1)		0.80(1)	
Ti backing (μm)	1 × 2.3(1)		3 × 2.3(1); 1 × 2.2(1)	
Experiment part	only run 1		run 1 and run 2	
Ti degrader (μm)	5.0(1)	5.5(1)	5.1(1)	5.6(1)
$\langle E_{\text{beam}}\rangle$[a] (MeV)	241.2	238.0	240.6	237.4
$E^*_{\text{CN,min}}$[b] (MeV)	34.7	32.1	35.7	33.1
$E^*_{\text{CN,max}}$[b] (MeV)	40.8	38.2	42.5	39.9
Beam integral (10^{18})	0.19(1)	0.26(2)	2.23(13)	3.29(19)
No. ^{286,288}Fl chains	2	–	6	5+1[c]
$\sigma(4n)$ (pb)[d]	$22(^{26}_{15})(3)$	–	$5.1(^{29}_{21})(6)$	$3.5(^{20}_{14})(4)$
No. ^{287,289}Fl chains	–	–	7	8
$\sigma(3n)$ (pb)[d]	–	–	$6.2(^{32}_{24})(8)$	$4.8(^{23}_{17})(6)$
σ(1 chain) (pb)[d]	$11(^{25}_{9})(1)$	$8(^{19}_{7})(1)$	$0.9(^{20}_{7})(1)$	$0.6(^{14}_{5})(1)$

[a]Energy losses were simulated with SRIM [48] and have ≈2 MeV systematic uncertainty.
[b]Masses of compound nuclei ^{290,292}Fl taken from [49].
[c]The ambiguous ^{286}Fl or ^{288}Fl chain was included here.
[d]Statistical and systematic uncertainties, corresponding to 1-σ confidence intervals, are given within the first and second parentheses, respectively.

Linear Accelerator (UNILAC) to an average intensity of 0.8 μA (particle) in relation to its pulsed beam structure, namely 5 ms beam on and 15 ms beam off. The beam was directed to the TASCA cave. Here, the accelerated ^{48}Ca ions collided with target layers of ^{242}Pu and ^{244}Pu, and flerovium nuclei were produced following fusion-evaporation reactions. The gas-filled recoil separator TASCA [50] was used to efficiently transmit, select, and focus the flerovium ions into an upgraded version of the TASISpec decay station [51,52]. Here, the structure of nuclei along the Fl-decay chains could be investigated by means of high-resolution particle-photon coincidence spectroscopy.

For the experiment, TASCA was filled with 0.8 mbar He gas [53]. The TASCA dipole magnet was set to center ions with magnetic rigidity $B\rho = 2.27$ Tm in the focal plane. This value had been established as an optimum value in previous studies of flerovium isotopes at GSI [7,8,42]. In 2019, prior to the first run of the main experiment, the reaction ^{48}Ca + ^{206,207}Pb was studied to ensure optimal asymmetric settings of the TASCA quadrupole magnets for the focusing into TASISpec, of which details are described in Ref. [52]. Another aspect of this start-up phase was investigating the use of a mixed target wheel loaded with two segments of ^{206}Pb and two segments of ^{207}Pb. Information from the TASCA control system concerning which target segment was irradiated at a given point in time [54] was correlated with implantation and decays of either ^{252}No or ^{253}No in the implantation detector of TASISpec. In the off line analysis it was found that this correlation does hold, but not on a sufficiently high level to unambiguously label a given implantation event with the correct target wheel segment [52].

For the main part of the experiment, isotopically enriched Pu material was electroplated onto 2.2 μm and 2.3 μm thick Ti foils creating four arc-shaped target segments [55]. The target segments were attached to a wheel such that the Ti backing foils faced the beam, and the target wheel rotated synchronously with the UNILAC's pulsed beam structure [54]. For the first run, one segment was composed of enriched ^{242}Pu, while the other three segments were composed of enriched ^{244}Pu. All four segments had 2.3(1) μm thick Ti backing foils. Because of the correlation problem indicated above, noted first after the 2019 part of the experiment (run 1), the target wheel was considered as one entity of 76.2% ^{244}Pu, 23.4% ^{242}Pu, 0.4% ^{240}Pu, plus negligible amounts of ^{238,239,241}Pu (<0.04%). Based on decay characteristics, two chains were assigned to ^{286}Fl, two to ^{288}Fl, and four to ^{289}Fl, while one remained ambiguous between ^{286}Fl or ^{288}Fl because of the missing full α-decay energy (cf. Refs. [20] and [46] and corresponding Supplemental Material).

For the second part of the main experiment (run 2), all four segments of the target wheel were composed of enriched ^{244}Pu backed by either 2.3(1) μm thick Ti foils (the same three segments as in run 1), or a 2.2(1) μm thick Ti foil (one segment). This wheel contained 98.5% ^{244}Pu, 1.1% ^{242}Pu, 0.4% ^{240}Pu, plus negligible amounts of ^{238,239,241}Pu (<0.04%). Nine more decay chains were associated with the production and decay of ^{288}Fl and 11 more chains with the production and decay of ^{289}Fl. Three more chains listed in Table I of the Supplemental Material [47] are candidates for ^{289}Fl decay chains, but considered ambiguous and therefore excluded from cross-section calculations as well as from all other analysis aspects. Details are presented in the Supplemental Material [47].

Over the course of the two experimental runs, a total beam integral of 6.0(4) × 10^{18} ions was collected. The 6.021(2) MeV/u ^{48}Ca beam was degraded with two different sets of Ti foils aiming to probe compound nucleus excitation energies around the anticipated peak of the 3n evaporation channel of the excitation functions [56]. The thicknesses of these foils, and resulting midtarget beam energies as well as compound nucleus excitation energies at the beginning and the end of the Pu target layer are presented in Table I. The last rows of the table present the cross sections for the 4n and 3n evaporation channels, corresponding to the creation of ^{286}Fl and ^{288}Fl, and ^{287}Fl and ^{289}Fl, respectively. Deduced cross sections are given separately for the different degrader thicknesses and target materials. For reference, the last row of the table provides the cross section corresponding to the observation of a single decay chain. In the cross-section calculations, transmission of Fl fusion-evaporation residues from the target into TASISpec was estimated to 30(3)% [57,58]. The identification efficiency of the Fl-decay chains were calculated based on decision trees to 90(3)% and 86(3)% for the 4n channel and 3n channel, respectively. These numbers take into account the number of members of the decay chain, expected number of random chains of a certain kind [47], missed events due to dead time within and outside the beam pulse [47], the efficiency for detecting α and spontaneous fission (SF) events with TASISpec [51], and the beam shut-off routine [56]. The cross-section values are associated with systematic uncertainties, which account for uncertainties in the beam integral, target thickness, transport efficiency as well as the identification efficiency. Statistical uncertainties are given in accordance to Ref. [59]. The resulting 3n and 4n channel cross sections in the ^{48}Ca + ^{244}Pu reaction agree well with those obtained in Refs. [13,42] and follow the typical shape of the excitation functions, see Fig. 4.5 in Ref. [56].

The recoiling flerovium ions were implanted into a 0.31-mm thick, 32 × 32-strip DSSD, denoted implantation DSSD. Charged particles were detected in the implantation DSSD as well as four additional 0.97 mm thick, 16 × 16-strip DSSDs placed upstream, denoted box DSSDs. Part of the TASISpec upgrade was a second 0.31-mm thick DSSD placed behind the implantation DSSD. Its main task was to veto unwanted background radiation from, for instance, low-energy signals during beam-off periods. It was therefore denoted veto DSSD [52]. The readout of the 256 preamplified DSSD channels was performed with 50-MHz, 14-bit sampling ADCs (see also Ref. [52]). 80-μs long traces were recorded. Five composite germanium detectors were placed closely behind each of the five sides of the DSSD cube. A seven-crystal cluster detector [60] was placed behind the implantation DSSD, while four novel four-crystal compex detectors [61] were positioned behind each of the box DSSDs. More information on the data processing of the germanium detectors is given in the Supplemental Material [47].

TABLE II. Reduced transition strengths, $B(\sigma L)$, and wave function overlaps, $\rho^2_{\rm fi}(E0)$ predicted from TBMF calculations [22,70], as well as tabulated internal conversion coefficients, $\alpha_{\rm tot}$, and $E0$ electronic factors, $\Omega_{\rm IP}$ [68,72–74], and derived transition rates, $\lambda(\sigma L)$, and branching ratios, br, for electromagnetic transitions between the states involved in the four decay scenarios of the excited state in ^{282}Cn (see Fig. 2). Lifetimes, τ, of states are based on the combined transition rates.

scenario	I_i^π	I_f^π	ΔE (MeV)	σL	$B(\sigma L)$ (W.u.)	$\alpha_{\rm tot}$	$\rho^2_{\rm fi}(E0)$ (10^{-3})	$\Omega_{\rm IP}$ (10^{12}/s)	$\lambda(\sigma L)$ (10^{12}/s)	br (%)	τ (ps)
(i)	0_2^+	0_1^+	0.62	$E0$			21.4	45.7	0.9771	98.3	1.01
	0_2^+	2_1^+	0.40	$E2$	9.09	0.3323			0.0167	1.7	
	2_1^+	0_1^+	0.22	$E2$	161	2.63			0.0405	100	24.7
(ii)	0_2^+	0_1^+	0.62	$E0$			21.4	45.7	0.9771	93.3	0.95
	0_2^+	2_1^+	0.55	$E2$	9.09	0.141			0.0703	6.7	
	2_1^+	0_1^+	0.07	$E2$	161	413			0.0151	100	66.4
(iii)	0_2^+	0_1^+	0.56	$E0$			21.4	43.3	0.9266	98.2	1.06
	0_2^+	2_1^+	0.40	$E2$	9.09	0.3323			0.0167	1.8	
	2_1^+	0_1^+	0.16	$E2$	161	9.746			0.0244	100	41.0
(iv)	2_2^+	2_1^+	0.40	$E0$			0.021	36.9	7.7×10^{-4}	0.3	3.9
				$M1$	1.7×10^{-6}	2.887			1.3×10^{-5}	0.0	
				$E2$	37.4	0.3323			0.0687	27.0	
	2_2^+	0_1^+	0.62	$E2$	13.6	0.106			0.1854	72.7	
	2_1^+	0_1^+	0.22	$E2$	161	2.63			0.0405	100	24.7

Two event types triggered the readout of the detector channels: (i) A p- or n-side strip of the implantation DSSD measured a signal above an energy threshold of ≈120 keV. (ii) An n-side strip of one of the box DSSDs measured a signal larger than ≈5 MeV. Depending on the actual beam intensity, accepted trigger rates were ≈1200 (≈150) events per second during beam-on (beam-off) periods.

During the 5-ms beam pulse of the UNILAC, background radiation levels are high, and, in particular, the germanium detectors are overloaded. Thus, for profound α-photon coincidence spectroscopy along the decay chains there is an impetus to do this during beam-off periods. Similarly, to establish the nonrandomness of Fl-decay chains, it is crucial to detect the terminating fission event within a beam-off period. This is particularly relevant for decay chains with either few α-decay steps, long correlation times, or both. Therefore, a so-called *beam shut-off routine* was implemented. Though, it is worth pointing out that for UNILAC beams there is in any case at least a 75% chance that the fission will occur during the beam-off periods. The principle of the shut-off routine is that upon the registration of a flerovium-like recoil-α correlation in the online data acquisition, an electrostatic chopper near the ion source was activated within 20 μs, preventing Ca-ions from being accelerated. This allowed for low-background measurements of subsequent decays up to 200 s (run 1) or 300 s (run 2). The TASCA control system allows to prolong the period by manual intervention of the experimenter on shift. Details of the implementation of the routine and its trigger conditions are described in Ref. [56]. The most important criterion was the detection of an $E_\alpha = [9.5, 10.3]$-MeV particle during the usual UNILAC beam-off period, for which the same pixel of the implantation DSSD was engaged by a preceding recoil candidate ($E_{\rm rec} = [11, 20]$ MeV) within $\Delta t < 20$ s. The routine accounted for neighboring-strip add-back as well as reconstructed implantation-box energies.

III. DATA ANALYSIS

The signals of implanted recoiling ions and of subsequent emissions of α particles or terminating spontaneous fission events in the same detector pixel served as a tagging technique in the identification of decay chains stemming from flerovium isotopes created in fusion-evaporation reactions. The search criteria, i.e., the energy and time windows, used to discriminate the correlated events related to flerovium decay chains, are presented in Table II in the Supplemental Material. They are identical to those used in determining the number of random chains as detailed in the Supplemental Material [47].

In total, a shy 44 beam-off fission events were registered throughout the three-week long experimental runs. All of these events were investigated in more detail by searching back in time for pixel-correlated recoil-implantation and decay signals resembling Fl-decay chains [56]. Thirty of these fission events are among the 32 candidate Fl-decay chains. Two decay chains were found to terminate with fission events detected during beam-on periods, namely chains 05 and 17 listed in the Supplemental Materials of Refs. [20,46], respectively. Additionally, 12 beam-off fission events were correlated with high-energy ($50 < E_{\rm rec} < 90$ MeV) transfer-reaction recoil implantation signals only a few milliseconds earlier. They are thus linked to short-lived fission isomers known in the actinide region. The remaining two beam-off fission events could not be correlated to an implantation event, most likely due to dead time of the data acquisition system (see Sec. I B in the Supplemental Material [47]).

Tables I in the Supplemental Materials of Refs. [20,46] as well as Table I in the Supplemental Material of this article [47] list a total of 32 candidates of decay chains based on the search parameters applied. The reasoning why chains 30, 31, and 32 were not associated with flerovium isotopes is outlined in Sec. I A in the Supplemental Material [47,62]. These three chains are *not* included in the following

analysis. The 29 correlated chains associated with a decay of a flerovium isotope comprise a total of 47 α-decay steps. Four recoil events were missing in the decay chains. A discussion of these, along with the missing α-decay steps, is subject of Sec. I B in the Supplemental Material [47]. The full energy of 30 α particles was measured in the implantation detector, ten events were reconstructed, three missed detection, and four escape events were listed, of which two were disregarded. Reconstructed and escape events are discussed in Sec. I C in the Supplemental Material [47,63]. Three photons were measured in the germanium detectors in prompt coincidence with the particles detected in the silicon detectors associated with the Fl decay chains and are further described in Sec. I E in the Supplemental Material [47,64,65].

Because of their relevance for the discussion later on, three observed α-electron coincidences are discussed in some detail. They were found in chain 2 for the α-decay step $^{286}\mathrm{Fl} \rightarrow {}^{282}\mathrm{Cn}$ [20] and in chains 26 and 27 for the α-decay step $^{285}\mathrm{Cn} \rightarrow {}^{281}\mathrm{Ds}$ [46], respectively. These coincidences are prompt, with $\Delta t < 50$ ns derived from the stored preamplifier pulses, between full-energy α-particle measurements in a pixel of the implantation detector, and low-energy electron signals detected in one of the box DSSD pixels. Note that in the cases of chain 2 and 27, these types of coincidences are not at all compatible with the concept of reconstructed α-particle events. For the case of chain 26 it is very unlikely ($\approx 10^{-3}$) as has been discussed in conjunction with Fig. 2(c) in the Supplemental Material [47]: α particles with low remaining energy would get stuck in the dead layer of either the implantation detector or, at the latest, the dead layer of the respective box DSSD.

To get a handle on the probability to observe prompt α-electron coincidences during beam-off periods, all such events detected throughout the complete experiment are shown in Fig. 1(a). Note that for this figure, the standard coincidence window of $\Delta t < 200$ ns was used, i.e., significantly larger than observed for the three events of interest.

Clearly, the α-electron coincidence spectrum in Fig. 1(a), as also seen in its projection on the α-energy axis in Fig. 1(b), is dominated by real correlations. The main peak measured at 8.78(1) MeV in Fig. 1(b) stems from the ground-state α decay of ^{212}Po, which has a half-life of only $T_{1/2} = 299(2)$ ns [66]. It is populated by β^- decay of ^{212}Bi. Its GEANT4 simulated spectrum, included in Fig. 1(b), is congruent with the experimental spectrum. Similarly, the peak at 8.38(1) MeV in Fig. 1(b) corresponds to the α decay of ^{213}Po, $T_{1/2} = 3.72(2)$ µs, preceded by the β^- decay of ^{213}Bi. The second nonrandom correlation scenario observed in Fig. 1 is a coincidence between an α decay and an internal conversion electron stemming from the electromagnetic transition of an excited state. The main contribution seen is the 6.28(1)-MeV α peak from ^{211}Bi, connecting with the 351-keV state in ^{207}Tl, the electromagnetic transition of which has a conversion coefficient of $\alpha_{\mathrm{tot}} = 0.243(4)$ [66]. In all cases observed and discussed above, depending on emission angle and actual decay energy of the electron, some part of its energy is summed with the α-particle and recoil energies in the implantation detector [67]. This gave rise to, e.g., the high-energy tail of the ^{212}Po α-decay peak which is reproduced well in the GEANT4 simulation.

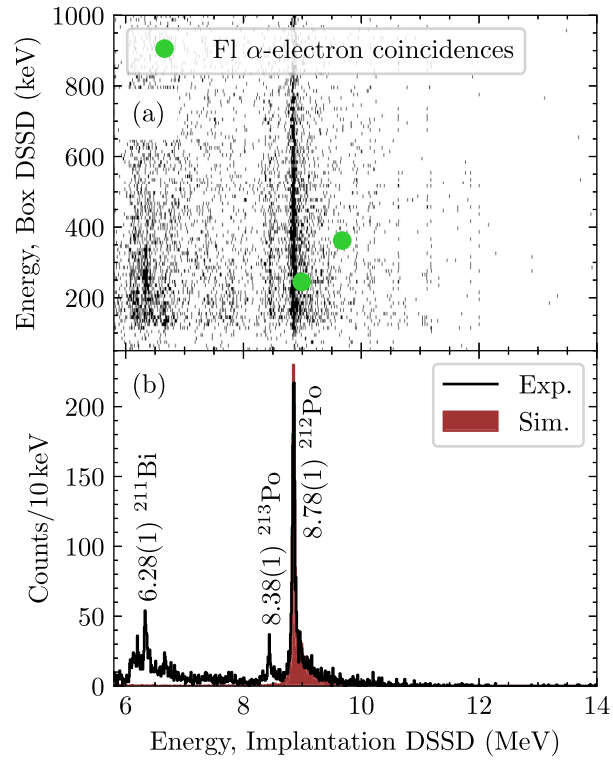

FIG. 1. (a) Energies of measured signals in prompt coincidence between the implantation detector (x axis) and any box DSSD (y axis) are visualized in a scatter plot. α-electron coincidences observed along the Fl α-decay chains are indicated. (b) Projection of the histogram in (a) onto the x axis with a binning of 10 keV per channel. Measured E_α for the three main peaks from ^{211}Bi, ^{213}Po, and ^{212}Po are labeled. GEANT4 simulation of ^{212}Bi is included. See text for details.

It is possible to identify the ^{211}Bi α-electron coincidences by means of a correlation analysis adapted for its α-decay chain. In contrast, this is not feasible for ^{212}Po nor ^{213}Po because of the too long half-lives of ^{213,212}Bi. Hence, if such an event was hypothetically observed within a Fl-decay chain, it would not be possible to establish that this event actually arose from decays of ^{212,213}Bi background. The ratio of the yield in the implantation detector spectrum that came with a prompt coincident signal within [50, 1000] keV in any of the box DSSDs, to the full implantation detector spectrum, in the range [8.5, 10.5] MeV, is on average 0.13. This means that about one in ten of the α decays measured in this range come in prompt coincidence with an electron. This is quite many, but the randomness of the event is, first and foremost, dictated by the probability to measure an α particle within [8.5, 10.5] MeV in the first place. For chains 2 and 27, i.e., those with α-electron coincidences as seen in Fig. 1(a), the probability to observe an α-decay event within [9.4, 10.5] MeV and [8.5, 9.5] MeV within the time period of the entire decay chains (0.054 s and 54.1 s) is 5×10^{-8} and 7×10^{-4}, respectively (see also Table II and Eq. (1) in Sec. I A in the Supplemental Material [47]). Thus, it is unlikely that these events stem from real background α-electron correlations.

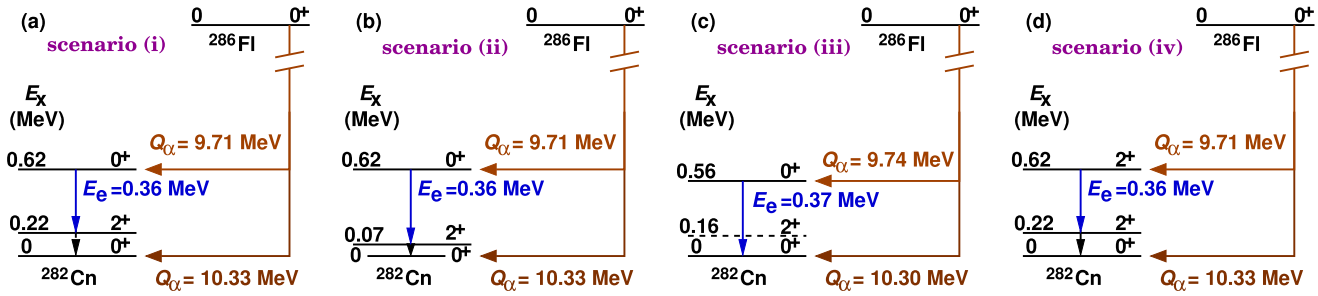

FIG. 2. Four decay scenarios, denoted (i)–(iv) in (a)–(d), of the excited state at $E_x \approx 0.6$ MeV in ^{282}Cn populated via the ^{286}Fl α decay. Indicated transitions, decay energies, and level energies were probed by GEANT4 simulations. The transitions associated with the measured $E_e = 0.36(1)$ MeV electron are marked in blue; they originate from an L-converted $E2$ transition in (a), a K-converted $E2$ transition in (b), a K-converted $E0$ transition in (c), or an L-converted, mixed $E2$, $M1$, or $E0$ transition in (d). See text for a detailed discussion.

For actual random box-electron coincidence estimates, induced purely by the rate of box-DSSD events, trigger rates in the [50,1000] keV range within the box DSSDs need to be monitored in future experiments. To mimic this and try to estimate the probability for such events, contributions from the identified α-electron coincidences were subtracted, i.e., fits to the three peaks identified in the spectrum in Fig. 1(b). The ratio of the yield here and the number of events in the full implantation detector spectrum within [6, 12] MeV was calculated resulting in a value of ≈0.01. Note that this value is a rather conservative upper limit, since many other non-random coincidences seen in Fig. 1 were *not* accounted for. Consequently, it was concluded that the probability of random electron coincidences in a box DSSD was <0.01.

IV. DISCUSSION

A. Decay of ^{282}Cn excited state

The detection of chain 02 marked the first observation of an excited state in the even-even nucleus ^{282}Cn. The experimental observations were described in detail and compared to predictions of contemporary triaxial beyond-mean-field (TBMF) calculations in Ref. [20]. The focus of the present work lies on investigating possible decay scenarios of the excited state in greater detail by confronting them with GEANT4 simulations and then comparing them with predicted transition strengths.

The ^{286}Fl α-decay event in chain 02 was measured to 9.60(1) MeV. The α particle was accompanied by a 0.36(1)-MeV electron, measured in prompt coincidence within $\Delta t <$ 50 ns, in one of the upstream box DSSDs Electron binding energies for the K and L shells in ^{282}Cn are ≈190 keV and ≈40 keV, respectively [68]. The measurements reported on the observation of a new α-decay branch of ^{286}Fl entering an excited state at $E_x \approx 0.6$ MeV in ^{282}Cn. For completeness, two neighboring germanium crystals detected a total of $E_\gamma = 205(1)$ keV, but 6.6 µs delayed with respect to the 9.60-MeV α-decay event. These germanium signals are disregarded in the analysis due to the expected number of randomly correlated delayed germanium hits (see Sec. I E in the Supplemental Material [47]).

Based on a hindrance factor for the 9.60 MeV α-decay branch of close to unity [20,69], the excited state in ^{282}Cn was suggested to have a spin-parity of $I^\pi = 0^+$. The extra hindrance expected due to angular momenta $\Delta\ell_\alpha \neq 0$ was further investigated using the superfluid tunneling model (STM) with the parameters introduced in Ref. [71]. Assuming $\ell_\alpha = 0$, the model predicts a partial decay width corresponding to $T_{1/2} \approx 9$ s. This compares well with the experimental partial half-life $T_{1/2}(\text{exp}) \approx 4$ s [20]. In the STM model, the extra hindrance expected for $\ell_\alpha = 2$ and $\ell_\alpha = 4$ yields $T_{1/2} \approx$ 13 s and $T_{1/2} \approx 32$ s, respectively. Since the predicted $T_{1/2}$ for $\ell_\alpha = 0$ is about the same as the predictions with $\ell_\alpha =$ 2, and because the predicted excitation energy of the 2_2^+ state in ^{282}Cn is $E_x = 0.79$ MeV [70], this option was also considered.

Altogether four different decay scenarios of the excited state are presented in Fig. 2, which relate to and focus on four different options for the origin of the observed electron coincidence. All panels provide the decay energies used for the GEANT4 simulations. The first scenario (i) corresponds to the tentative scenario originally considered most likely in Ref. [20]. Here, the measured conversion electron stems from the L shell, i.e., from an L-converted 0.40 MeV, $0_2^+ \rightarrow 2_1^+$, $E2$ transition. The ground state is reached through another highly converted 0.22-MeV $E2$ transition. A $Q_\alpha = 9.71$ MeV has been deduced assuming a possible 0.03-MeV electron summing from atomic relaxation processes [20], and employing $Q_\alpha = 10.33$ MeV from all hitherto observed ^{286}Fl decay chains, as described in the Supplemental Material of Ref. [20]. The second scenario (ii) is essentially the same as scenario (i), except that the measured conversion electron is assumed to stem from the K shell of a 0.55-MeV $E2$ transition. The ground state is now reached through another $E2$ transition of 0.07 MeV.

In the third scenario (iii), the conversion electron is considered to stem from the K shell of a 0.56 MeV, $0_2^+ \rightarrow 0_1^+$, $E0$ transition, which proceeds directly to the ground state, thereby passing the 2_1^+ state predicted at $E_x = 0.16$ MeV [70]. However, the energies in this scenario must be adjusted: for the ground-state to ground-state decay, $Q_\alpha =$ 10.30 is derived from the measured E_α of chain 01 from the current experiment. This value corresponds to the 1-σ endpoint for the energy of this branch, $Q_\alpha = 10.33(3)$ MeV, compiled from current and previous experiments [20]. Similarly, assuming a measured electron energy of $E_e = (0.36 +$ 0.01) MeV = 0.37 MeV, the excitation energy of the 0_2^+ state becomes 0.56 MeV, populated by α particles consistent with

$E_\alpha = 9.60(1)$ MeV, i.e., the experimental value of chain 02. With these assumptions, the decay energies of scenario (iii) are consistent with the experimental observations.

Finally, the fourth decay scenario (iv) is the same as scenario (i), but with spin $I^\pi = 2^+$ proposed for the level at 0.62 MeV. Here, the 0.36-MeV electron originates from an L-converted, 0.40-MeV, $2_2^+ \rightarrow 2_1^+$ transition, which can be of $E2$, $M1$, or $E0$ character. Like scenario (i), the ground state is reached through a highly converted 0.22-MeV $E2$ transition.

Table II summarizes the numbers used for the GEANT4 simulations and subsequent discussion of the four decay scenarios. Total conversion coefficients, $\alpha_{\rm tot}$, and $E0$ electronics factors, $\Omega_{\rm IP}$, were taken from Refs. [68,72,73] and cross-checked [74]. Reduced transition strengths were calculated with state-of-the-art TBMF calculations [22,70] performed with the Gogny force using the D1S parametrization [75], for all transitions connecting the potentially involved 0_1^+, 0_2^+, 2_1^+, and 2_2^+ states. The monopole strengths were calculated to $\rho^2(E0) \approx 2 \times 10^{-2}$ and 2×10^{-5} for the $0_2^+ \rightarrow 0_1^+$ $E0$ transition and $2_2^+ \rightarrow 2_1^+$ $E0$ contribution, respectively.

The virtual TASISpec experimental setup [15] was first modified to accommodate relevant updates of the decay station [52]. Then, simulated data was processed with the same analysis code as the experimental data [56]. Decay data were set to match the energies for a given scenario as indicated in Fig. 2. Internal conversion coefficients are listed in Table II. Note that, from the GEANT4 perspective, scenarios 1 and 4 deliver practically identical simulated spectra, because the 0.40-MeV transition has (essentially) pure $E2$ character in both cases.

Figure 3 compares experimental spectra with simulated spectra for the implantation DSSD, the coincidences in the box DSSDs, and coincidences with the germanium detectors. The simulated spectra were normalized to the *one*α-decay event detected at 9.6 MeV, i.e., the implantation DSSD spectrum integral within [9.55, 9.65] MeV. From the implantation-DSSD spectrum in Fig. 3(a), the assumed electron summing of 0.03(2) MeV, seems to match best with the experimental point in the case of scenario (ii). For scenarios (i) and (iv), an increase of the Q value of the decay into the excited state by some 20–30 keV could solve the discrepancy in the peak position near 9.6 MeV. Such a small shift in energy can be accounted for within the experimental uncertainties. For scenario (iii), however, a corresponding decrease of that Q value would require to stretch the experimental energies beyond their 1-σ uncertainty range (see above).

The box-DSSD coincidence spectra in Fig. 3(b) are most relevant for the current experimental observations. It is clear that scenario (iii) is by far the scenario which provides the highest probability for a coincident 0.36(1)-MeV conversion electron. For this scenario, one count in the 0.36-MeV box-DSSD coincidence peak is expected in about 16% of the cases when the α decay enters the ≈0.6 MeV excited state. For scenarios (i),(iv) and (ii), corresponding numbers are only 3% and 1%, respectively.

Though, unfortunately unobserved for the current α-decay event, a coincident K x ray or γ ray would be very helpful to distinguish between the different scenarios. It can be seen in Fig. 3(c) that K x rays are dominating the photon spectrum of scenario (iii). In fact, the detection of a K x ray is expected in about 30% of the cases when the ≈0.6 MeV state decays. At variance, the photon spectra of scenarios (i),(iv) and (ii) are dominated by 0.22- and 0.40-MeV or 0.55-MeV γ rays and their detection is expected in 10%, 18%, and 16% of the cases, respectively.

The predictions from the comprehensive TBMF nuclear structure calculations (cf. Table II) strongly favor the $0_2^+ \rightarrow 0_1^+$ $E0$ branch (br > 90%) over the $E2$-$E2$ cascade via the

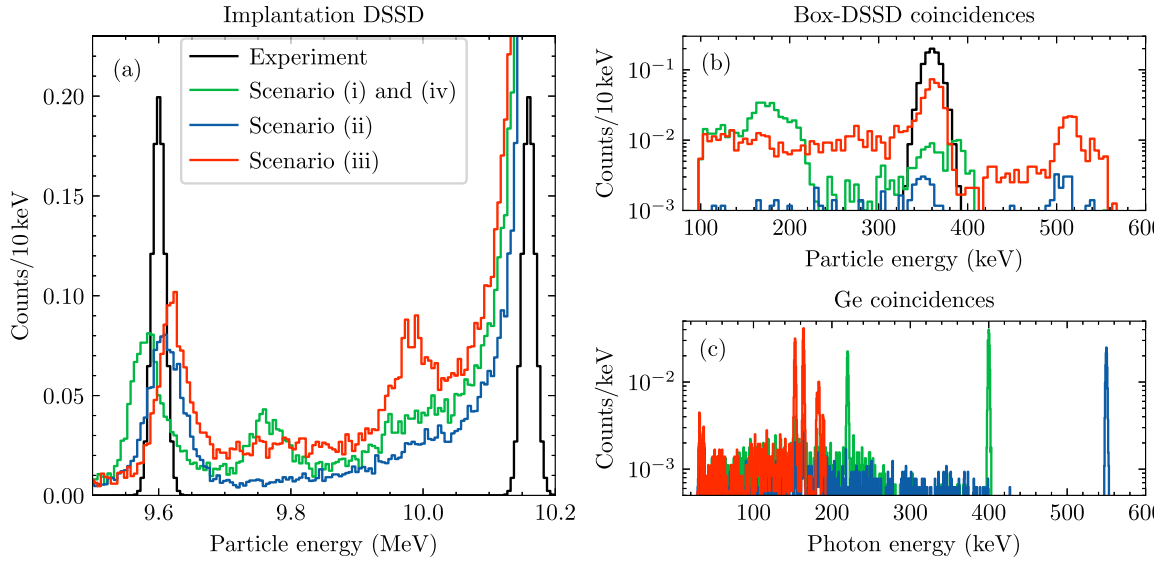

FIG. 3. Experiment and GEANT4 simulated particle implantation DSSD (a), box-DSSD coincidence (b), and photon coincidence (c) spectra for the ^{286}Fl decay scenarios introduced in Fig. 2. Experimental data points are represented with a Gaussian of integral one and a width compliant with its measured systematical uncertainty. Simulated data are normalized to the implantation DSSD spectrum integral within [9.55, 9.65] MeV.

TABLE III. Summary of measured and predicted spontaneous fission characteristics of even-even isotopes in the observable triangle ^{284}Fl - ^{290}Fl - ^{278}Hs. Chain 17 detailed in Table I in the Supplemental Material of Ref. [46] is presumed to start from ^{290}Fl. Branching ratios (br) are given in percent.

Isotope	experiment						$T_{1/2,\mathrm{SF}}$, theoretical			
	Ref.	#[a]	$T_{1/2}$	br$_\alpha$	br$_{\mathrm{SF}}$	$T_{1/2,\mathrm{SF}}$	MM-WS [79,80]	MM-FRLDM ($\times 10^{-8}$)[b]	DFT-SKM* ($\times 10^{6}$) [86]	HFB-TRI-OCT [b]
^{284}Fl	[44]	5	$2.5(^{18}_{8})$ ms	$\leqslant 17$	100	$2.5(^{18}_{8})$ ms	12 ms	0.9 s	0.5 ms	3 ms
^{286}Fl	[20][c]	29	$0.121(^{31}_{21})$ s	55	45	$0.27(^{7}_{5})$ s	1.5 s	30 s	30 ms	3.4 s
^{288}Fl	[20][c]	47	$0.65(^{12}_{8})$ s	100	$\leqslant 2$	>28 s	2100 s	47 s	8.7 s	21 s
^{282}Cn	[20][c]	17	$0.98(^{33}_{20})$ ms	$\leqslant 6$	100	$0.98(^{33}_{20})$ ms	71 ms	0.4 ms	9 ms	0.3 ms
^{284}Cn	[20][c]	51[d]	$0.121(^{20}_{15})$ s	2	98	$0.123(^{20}_{15})$ s	4.0 s	0.1 s	0.7 ms	0.2 s
^{280}Ds	[20][c]	1	$0.36(^{172}_{16})$ ms	$\leqslant 50$	100	$0.36(^{172}_{16})$ ms	12 ms	1 µs	30 ms	
(^{290}Fl)		1	$0.31(^{148}_{14})$ s	100	$\leqslant 50$	>0.34 s	4.3 d	4 d	10 h	0.1 s
(^{286}Cn)		1	$19(^{91}_{8})$ s	100	$\leqslant 50$	>22 s	1920 s	0.2 s	0.22 s	30 ms
(^{282}Ds)		1	$35(^{165}_{15})$ s	$\leqslant 50$	100	$35(^{165}_{15})$ s	1.5 s	0.4 ms	0.05 ms	3 ms

[a]Total number of observed nuclei.
[b]Calculations are described in text.
[c]See Table II in the Supplemental Material of Ref. [20] for a combined assessment of all hitherto measured decay energies and correlation times for decay chains involving ^{286,288}Fl.
[d]Data on ^{284}Cn includes four decay chains from element 114 chemistry experiments behind TASCA [7,8].

2_1^+ state for the concerned scenarios (i)–(iii). This is because of a rather large overlap of wave functions despite a shape-changing transition, $\rho^2_{\mathrm{fi}} \approx 20 \times 10^{-3}$, which multiplied by a large ('superheavy') electronic factor of $\Omega_{\mathrm{IP}} \approx 4.5 \times 10^{13}$/s leads to a (partial) lifetime of $\tau \approx 1$ ps for the 0_2^+ state. The competing $E2$ transition is about 50 times slower. Similarly, for scenario (iv), the 0.62-MeV $2_2^+ \rightarrow 0_1^+$ ground-state decay branch dominates the 0.40-MeV $2_2^+ \rightarrow 2_1^+$ branch, which in addition has only a rather small probability for internal conversion. Thus, the TBMF predictions are hardly compatible with scenarios (i), (ii), and (iv), i.e., the most probable solution is that the electron from the observed α-e^- coincidence event is a K-conversion electron from an $E0$ transition connecting a 0_2^+ state at an excitation energy $E_x \approx 0.60$ MeV to the ground state.

Finally, all predicted lifetimes, $\tau < 100$ ps, are consistent with experimentally observed or expected prompt coincidences between the α particle and the emitted electromagnetic radiation.

B. Decay probabilities

Chain 08 detailed in Table I in the Supplemental Material of Ref. [20] marked the first observation of a firm full-energy α decay from ^{284}Cn, and consequently the discovery of ^{280}Ds along with its spontaneous fission (SF) decay. The α decay from ^{284}Cn was thoroughly discussed in Ref. [20]. Therefore, the SF decay of ^{280}Ds is addressed in the present work. In combination with updated values for ^{286}Fl, ^{282}Cn, and ^{284}Cn, the new data point, i.e., for the SF half-life of ^{280}Ds, $T_{1/2,\mathrm{SF}}$, prompts comparison to theoretical calculations. In this discussion, the option that decay chain 17 detailed in Table I in the Supplemental Material of Ref. [46], observed in the present experiment, possibly starting from ^{290}Fl, is included. This decay chain is difficult to combine with the majority of the decay chains assigned to ^{289}Fl in a common decay scheme [46]. The decay branch marked 'low' in Ref. [46] is another option, but it is not considered here. Another peculiar decay chain, observed in a different experiment and originally assigned to ^{289}Fl [29], was critically assessed in, for instance, Refs. [31,32], and it is not further discussed here.

Experimental numbers are summarized in Table III, and the experimental $T_{1/2,\mathrm{SF}}$ values are compared to a number of predictions. Irrespective of the underlying nuclear structure model, calculating fission half-lives was, and is, a complex problem. Because of the necessary extrapolations, this is particularly true for the superheavy element regime, while increasingly reliable experimental values emerge. A recent theoretical overview of achievements and persisting issues for various theoretical approaches is given in Ref. [76]. Reference [77] surveys SF properties of heavy and superheavy nuclei from the experimental perspective. A contemporary semiempirical approach has recently been put forward in Ref. [78].

The macroscopic-microscopic predictions based on a Woods-Saxon potential, MM-WS, from Refs. [79,80], which are also used in, for instance, Refs. [32,77], are listed first in Table III. Despite the restriction to axial shapes, the predictions are rather close to the observed values, namely within one order of magnitude for Fl isotopes, and within two orders of magnitude for Cn and Ds, respectively. As such, it is reasonable to confront the candidate ^{290}Fl-decay chain with the MM-WS predictions. It is noted that the deviation is always in the upper direction for the known cases, but in the opposite direction for ^{282}Ds, i.e., the isotope concluding the considered option of a ^{290}Fl-decay chain. Assuming the same ratio between the observed and calculated values for ^{282}Ds as for ^{280}Ds and ^{284}Cn, one would have expected an experimental $T_{1/2,\mathrm{SF}}(^{282}\mathrm{Ds}) \approx 1.5\,\mathrm{s}/30 = 50$ ms, which is about 700 times less than the observed value for chain 17. The estimate thus disfavors an assignment of this option to chains originating from ^{290}Fl. A deficiency of the macroscopic-microscopic model relates to α-decay probabilities; for all Fl and Cn iso-

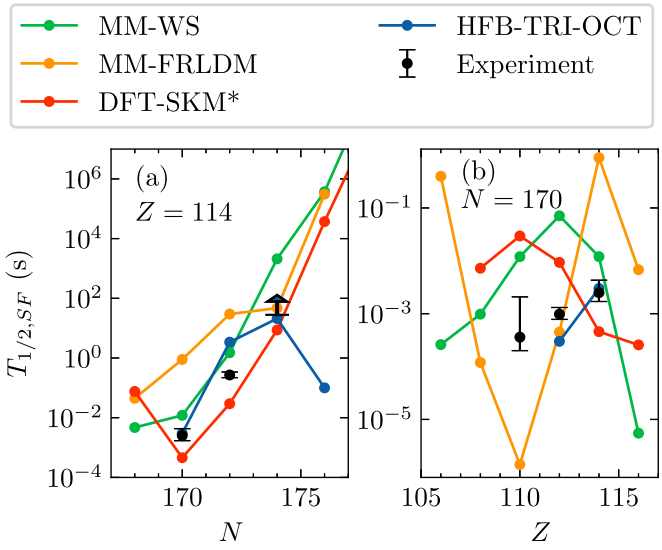

FIG. 4. Experimental and theoretical spontaneous fission half-lives, $T_{1/2,\mathrm{SF}}$, for even-even nuclei at $Z = 114$ vs. neutron number (a) and at $N = 170$ vs. proton number (b). Predicted numbers stem from MM-WS [79,80], DFT-SKM* [86] together with the MM-FRLDM and HFB-TRI-OCT calculations that are described in the text.

topes listed in Table III, the α-decay branch is predicted to dominate, at variance with the observations.

The second set of predicted values in Table III is based on the macroscopic-microscopic finite-range liquid-drop model (MM-FRLDM) [81]. This model employs axially symmetric shapes within the five-dimensional three-quadratic-surface parametrization. Dynamical fission calculations based on this model recently predicted a region of very asymmetric compact fission centered at $Z = 110$ and $N = 170$ [82]. The half-lives are calculated with the WKB formalism as in Ref. [83]. The water-immersion method [81] is used to obtain the fission path for the asymmetric fission, which is the dominant mode in the calculations in this region. The inertial mass is calculated with the semiempirical formula used in Ref. [83] for the compact fission path in fermium. Here, the asymptotic value corresponding to the reduced mass of the two fragments is reached when the neck radius along the fission path rapidly shrinks to a small value ($c_0 < 2.5$ fm [84]). Both MM-WS and MM-FRLDM give large fission-barrier heights, and thus large values of the half-lives, around $^{270}_{108}\mathrm{Hs}_{162}$ and $^{298}_{114}\mathrm{Fl}_{184}$. It is interesting to note that the region in between these two cases roughly coincides with the predicted compact asymmetric fission, resulting in a reduction of the lifetimes. The MM-FRLDM predicts much higher barriers in this region than MM-WS, as discussed in Ref. [85]. For a qualitative half-life comparison, the values in Table III and Fig. 4 were scaled by a factor 10^{-8}.

The third set of predicted values in Table III is "based on self-consistent symmetry-unrestricted nuclear density functional theory" (SkM* functional) [86]. While the model and its parameters were able to provide good predictions for SF of lighter and more neutron-deficient heavy and superheavy nuclei, extrapolation toward the superheavy isotopes of interest here, was found too steep (see also Ref. [77]). Note that in Table III and Fig. 4, $T_{1/2,\mathrm{SF}}$ was scaled up by six orders of magnitude to match the experimental values.

Finally, the last set of theoretical calculations, denoted HFB-TRI-OCT, represents the results based on the self-consistent constrained Hartree-Fock-Bogoliubov (HFB) theory [87]. In the present approach, the HFB equations are solved without restrictions on octupole and triaxial shapes along the fission path taking the operator Q_{20} as constraint. The present calculations are a generalization of those by Warda and Egido [88], where either axially symmetric octupole shapes or plain triaxial shapes (without octupole deformation) were allowed. Now, both octupole and triaxial shapes are considered simultaneously in the energy minimization process, see also Ref. [89]. This is a significant improvement because it is well known that triaxial shapes are relevant on the way to and at the first barrier while octupole shapes are important around the second barrier. In the calculations, the finite-range density-dependent Gogny force [75] in its D1S parametrization is used with a configuration space of 21 major shells.

Figure 4 compares experimental and theoretical spontaneous fission half-lives. For the flerovium isotopes ($Z = 114$), displayed in panel (a), the experimental values are seen to increase exponentially with larger neutron number. As expected from the increased stability as the anticipated $N = 184$ magic number is approached. This trend is also seen in all theoretical predictions, except for the HFB-TRI-OCT. While these predictions agree very well with the experimental data, a slightly lower half-life for $^{290}_{114}\mathrm{Fl}_{176}$ breaks the trend. The experimental $T_{1/2,\mathrm{SF}}$ values along the $N = 170$ isotonic chain in Fig. 4(b) are also exponentially increasing, albeit less pronounced. The MM-WS, MM-FRLDM, and DFT-SKM* predictions all show a peak, but at different proton numbers. The HFB-TRI-OCT predictions again show a remarkably good agreement with the experimental data points. At first glance, the comparison in Fig. 4(b) seems intriguing. However, the theoretical predictions are associated with significant uncertainties [76]. Consequently, more reliable theoretical predictions are required to reach sensitivities to properly assess subtle trends such as that of the $N = 170$ isotonic chain. The HFB-TRI-OCT calculations show potential in closing the large gap between theory and experiment with regards for spontaneous fission half-lives of superheavy nuclei.

V. CONCLUDING REMARKS

A nuclear spectroscopy experiment to study flerovium decay chains was conducted at the GSI Darmstadt, Germany. Among experimental details described, the use of a target wheel with mixed ^{242,244}Pu segments was emphasized. Due to impaired means to determine the hit target segment, it was concluded that isotope assignment had to rely on observed decay characteristics for the first part of the experiment.

Analysis and statistical assessments of the data set have been detailed. They led to 32 candidate Fl-decay chains, of which 29 were firmly assigned to stem from the production of a flerovium isotope, as summarized in Tables I in the Supplemental Materials of Refs. [20,46].

Because of the rather long decay times of ^{288,289}Fl, the importance of using a beam shut-off routine was demonstrated for this type of implantation-decay experiment, in combination with the unique advantages of the pulsed UNILAC beam.

By investigating event rates and the system dead time, the expected number of random chains and photon coincidence rates was determined. This allowed for missing events to be explained, three candidate chains to be disregarded due to their relative randomness, and randomly correlated photons to be quantified. The decay chains include six escape-α events. GEANT4 simulations, combined with rates of random background events, aided their interpretations and consequently two of the six events were disregarded. Three of the α-decay events came in prompt coincidence with electrons depositing their energies in one of the box DSSDs. The random probability for these events, which are of specific interest to unravel the nuclear structure of superheavy nuclei, was determined to <0.01. A method to describe the measured fraction of the recoiling energy of the implanted α-decaying nucleus is presented, building on well-known α-decay energies of nonfusion and calibration-reaction products. Having the recoil fraction parameter under control for a given setup is essential for the determination of precise α energies.

Based on GEANT4 simulations and predicted reduced transition strengths, four decay scenarios of the excited state found at $E_x \approx 0.6$ MeV in ^{282}Cn were investigated. With this analysis, superheavy nuclear spectroscopy has been pushed to its current limit. Further high-sensitivity multicoincidence spectroscopy measurements show potential to pinpoint the decay of the excited state.

Finally, experimental decay probabilities of even-even isotopes in the region of Fl-decay chains were compared to theoretically predicted spontaneous fission half-lives. Contemporary 'self-consistent Hartree-Fock-Bogoliubov' based calculations, including both triaxial and octupole shapes, show potential in closing the large gap between theory and experiment with regards to spontaneous fission half-lives of superheavy nuclei. Here, the optional assignment of one Fl-decay chain to start from ^{290}Fl was also presented but disfavored based on the lifetime of the terminating fission. Mass or mass-number resolved spectroscopy experiments are being called for to identify the most neutron-rich $Z = 114$ (^{290}Fl) and $Z = 116$ (^{294}Lv) isotopes accessible in ^{48}Ca-induced fusion reactions.

ACKNOWLEDGMENTS

The results presented here are based on the experiment U310, which was performed at the beam line X8/TASCA at the GSI Helmholtzzentrum für Schwerionenforschung, Darmstadt (Germany) in the frame of FAIR Phase-0. The authors would like to thank the ion-source and accelerator staff at GSI for their supreme efforts. This work has received funding from the European Union's Horizon 2020 research and innovation programme under Grant Agreement No. 654002 (ENSAR2). The ^{244}Pu target material was provided by the U.S. DOE through ORNL. The Lund group is indebted to decisive support from the Knut and Alice Wallenberg foundation (KAW 2015.0021), and we highly appreciate the possibility to collaborate with the workshops at IKP Köln. This work was also supported by the Swedish Research Council (Vetenskapsrådet, VR 2016-3969), the Royal Physiographic Society in Lund, the Spanish Ministerio de Ciencia e Inovación under Contract No. FPA2017-84756-C4-2-P, the German BMBF (05P18UMFN2), the U.S. DOE under Contract No. DE-AC02-05CH11231 (LBNL), and the UK STFC. A.S.-R., D.M.C., and D.R. are grateful for discussions with A. Jungclaus, CSIC Madrid, and support from T. Kibédi, ANU, Canberra.

[1] L. Öhrström and J. Reedijk, Pure Appl. Chem. **88**, 1225 (2016).
[2] Y. Ts. Oganessian and V. K. Utyonkov, Nucl. Phys. A **944**, 62 (2015).
[3] C. E. Düllmann, EPJ Web Conf. **131**, 08004 (2016).
[4] J. Khuyagbaatar, A. Yakushev, C. E. Düllmann, D. Ackermann, L.-L. Andersson, M. Asai *et al.*, Phys. Rev. C **102**, 064602 (2020).
[5] A. Türler, R. Eichler, and A. Yakushev, Nucl. Phys. A **944**, 640 (2015).
[6] A. Yakushev and R. Eichler, EPJ Web Conf. **131**, 07003 (2016).
[7] A. Yakushev, J. M. Gates, A. Türler, M. Schädel, C. E. Düllmann, D. Ackermann *et al.*, Inorg. Chem. **53**, 1624 (2014).
[8] A. Yakushev, L. Lens, C. E. Düllmann, J. Khuyagbaatar, E. Jäger, J. Krier *et al.*, Front. Chem. **10**, 976635 (2022).
[9] D. Ackermann, Nucl. Phys. A **944**, 376 (2015).
[10] D. Rudolph, U. Forsberg, P. Golubev, L. G. Sarmiento, A. Yakushev, L.-L. Andersson *et al.*, Phys. Rev. Lett. **111**, 112502 (2013).
[11] J. M. Gates, K. E. Gregorich, O. R. Gothe, E. C. Uribe, G. K. Pang, D. L. Bleuel *et al.*, Phys. Rev. C **92**, 021301(R) (2015).
[12] U. Forsberg, D. Rudolph, L.-L. Andersson, A. Di Nitto, C. E. Düllmann, C. Fahlander *et al.*, Nucl. Phys. A **953**, 117 (2016).
[13] C. E. Düllmann, M. Schädel, A. Yakushev, A. Türler, K. Eberhardt, J. V. Kratz *et al.*, Phys. Rev. Lett. **104**, 252701 (2010).
[14] Y. Shi, D. E. Ward, B. G. Carlsson, J. Dobaczewski, W. Nazarewicz, I. Ragnarsson, and D. Rudolph, Phys. Rev. C **90**, 014308 (2014).
[15] L. G. Sarmiento, L.-L. Andersson, and D. Rudolph, Nucl. Instrum. Methods Phys. Res. A **667**, 26 (2012).
[16] D. Rudolph, L. G. Sarmiento, and U. Forsberg, AIP Conf. Proc. **1681**, 030015 (2015).
[17] L. G. Sarmiento, EPJ Web Conf. **131**, 05004 (2016).
[18] J. Dobaczewski, A. V. Afanasjev, M. Bender, L. M. Robledo, and Y. Shi, Nucl. Phys. A **944**, 388 (2015).
[19] P.-H. Heenen, J. Skalski, A. Staszczak, and D. Vretenar, Nucl. Phys. A **944**, 415 (2015).
[20] A. Såmark-Roth, D. M. Cox, D. Rudolph, L. G. Sarmiento, B. G. Carlsson, J. L. Egido *et al.*, Phys. Rev. Lett. **126**, 032503 (2021).

[21] S. Ćwiok, P.-H. Heenen, and W. Nazarewicz, Nature (London) **433**, 705 (2005).

[22] J. L. Egido and A. Jungclaus, Phys. Rev. Lett. **125**, 192504 (2020).

[23] S. Ćwiok, W. Nazarewicz, and P. H. Heenen, Phys. Rev. Lett. **83**, 1108 (1999).

[24] A. Parkhomenko and A. Sobiczewski, Acta Phys. Pol. B **36**, 3115 (2005).

[25] S. Hofmann, S. Heinz, R. Mann, J. Maurer, J. Khuyagbaatar, D. Ackermann *et al.*, Eur. Phys. J. A **48**, 62 (2012).

[26] A. N. Kuzmina, G. G. Adamian, and N. V. Antonenko, Phys. Rev. C **85**, 027308 (2012).

[27] P. Jachimowicz, M. Kowal, and J. Skalski, Phys. Rev. C **89**, 024304 (2014).

[28] C. E. Bemis, Jr., R. J. Silva, D. C. Hensley, O. L. Keller, Jr., J. R. Tarrant, L. D. Hunt, P. F. Dittner, R. L. Hahn, and C. D. Goodman, Phys. Rev. Lett. **31**, 647 (1973).

[29] Y. Ts. Oganessian, V. K. Utyonkov, Y. V. Lobanov, F. Sh. Abdullin, A. N. Polyakov, I. V. Shirokovsky *et al.*, Phys. Rev. Lett. **83**, 3154 (1999).

[30] Y. Ts. Oganessian, A. V. Yeremin, A. G. Popeko, S. L. Bogomolov, G. V. Buklanov, M. L. Chelnokov *et al.*, Nature (London) **400**, 242 (1999).

[31] F. P. Heßberger, Chem. Phys. Chem. **14**, 483 (2013).

[32] S. Hofmann, S. Heinz, R. Mann, J. Maurer, G. Münzenberg, S. Antalic *et al.*, Eur. Phys. J. A **52**, 180 (2016).

[33] Y. Ts. Oganessian, J. Phys. G **34**, R165 (2007).

[34] Y. Ts. Oganessian, V. K. Utyonkov, Y. V. Lobanov, F. Sh. Abdullin, A. N. Polyakov, I. V. Shirokovsky *et al.*, Phys. Rev. C **62**, 041604(R) (2000).

[35] Y. Ts. Oganessian, V. K. Utyonkov, Y. V. Lobanov, F. Sh. Abdullin, A. N. Polyakov, I. V. Shirokovsky *et al.*, Phys. Rev. C **63**, 011301(R) (2000).

[36] Y. Ts. Oganessian, V. K. Utyonkov, Y. V. Lobanov, F. Sh. Abdullin, A. N. Polyakov, I. V. Shirokovsky *et al.*, Phys. Rev. C **70**, 064609 (2004).

[37] Y. Ts. Oganessian, V. K. Utyonkov, Y. V. Lobanov, F. Sh. Abdullin, A. N. Polyakov, I. V. Shirokovsky *et al.*, Phys. Rev. C **69**, 054607 (2004).

[38] Y. Ts. Oganessian, V. K. Utyonkov, Y. V. Lobanov, F. Sh. Abdullin, A. N. Polyakov, R. N. Sagaidak *et al.*, Phys. Rev. C **74**, 044602 (2006).

[39] S. Hofmann, D. Ackermann, S. Antalic, H. G. Burkhard, V. F. Comas, R. Dressler *et al.*, Eur. Phys. J. A **32**, 251 (2007).

[40] L. Stavsetra, K. E. Gregorich, J. Dvorak, P. A. Ellison, I. Dragojević, M. A. Garcia, and H. Nitsche, Phys. Rev. Lett. **103**, 132502 (2009).

[41] P. A. Ellison, K. E. Gregorich, J. S. Berryman, D. L. Bleuel, R. M. Clark, I. Dragojević *et al.*, Phys. Rev. Lett. **105**, 182701 (2010).

[42] J. M. Gates, C. E. Düllmann, M. Schädel, A. Yakushev, A. Türler, K. Eberhardt *et al.*, Phys. Rev. C **83**, 054618 (2011).

[43] Y. Ts. Oganessian, F. Sh. Abdullin, C. Alexander, J. Binder, R. A. Boll, S. N. Dmitriev *et al.*, Phys. Rev. Lett. **109**, 162501 (2012).

[44] V. K. Utyonkov, N. T. Brewer, Y. Ts. Oganessian, K. P. Rykaczewski, F. Sh. Abdullin, S. N. Dmitriev *et al.*, Phys. Rev. C **92**, 034609 (2015).

[45] D. Kaji, K. Morita, K. Morimoto, H. Haba, M. Asai, K. Fujita *et al.*, J. Phys. Soc. Jpn. **86**, 034201 (2017).

[46] D. M. Cox, A. Såmark-Roth, D. Rudolph, L. G. Sarmiento, R. M. Clark, J. L. Egido, P. Golubev, J. Heery, A. Yakushev, S. Åberg *et al.*, Phys. Rev. C **107**, L021301 (2023).

[47] See Supplemental Material at http://link.aps.org/supplemental/10.1103/PhysRevC.107.024301 for more details of the data analysis procedures and assessments concerning decay chains (not) associated with flerovium isotopes.

[48] J. F. Ziegler, Nucl. Instrum. Methods Phys. Res. B **219–220**, 1027 (2004).

[49] W. D. Myers and W. J. Swiatecki, Nucl. Phys. A **601**, 141 (1996).

[50] A. Semchenkov, W. Brüchle, E. Jäger, E. Schimpf, M. Schädel, C. Mühle *et al.*, Nucl. Instrum. Methods Phys. Res. B **266**, 4153 (2008).

[51] L.-L. Andersson, D. Rudolph, P. Golubev, R.-D. Herzberg, R. Hoischen, E. Merchán *et al.*, Nucl. Instrum. Methods Phys. Res. A **622**, 164 (2010).

[52] D. M. Cox, A. Såmark-Roth, D. Rudolph, L. G. Sarmiento, C. Fahlander, U. Forsberg *et al.*, J. Phys.: Conf. Ser. **1643**, 012125 (2020).

[53] J. Khuyagbaatar, D. Ackermann, L.-L. Andersson, J. Ballof, W. Brüchle, C. E. Düllmann *et al.*, Nucl. Instrum. Methods Phys. Res. A **689**, 40 (2012).

[54] E. Jäger, H. Brand, C. E. Düllmann, J. Khuyagbaatar, J. Krier, M. Schädel, T. Torres, and A. Yakushev, J. Radioanal. Rad. Nucl. Chem. **299**, 1073 (2014).

[55] J. Runke, C. E. Düllmann, K. Eberhardt, P. A. Ellison, K. E. Gregorich, S. Hofmann *et al.*, J. Radioanal. Rad. Nucl. Chem. **299**, 1081 (2014).

[56] A. Såmark-Roth, Spectroscopy along decay chains of element 114, Flerovium, Ph.D. thesis, Lund University, 2021.

[57] U. Forsberg, P. Golubev, L. G. Sarmiento, J. Jeppsson, D. Rudolph, L.-L. Andersson *et al.*, Acta Phys. Pol. B **43**, 305 (2012).

[58] K. E. Gregorich, Nucl. Instrum. Methods Phys. Res. A **711**, 47 (2013).

[59] K.-H. Schmidt, C.-C. Sahm, K. Pielenz, and H.-G. Clerc, Z. Phys. A **316**, 19 (1984).

[60] J. Eberth, H. G. Thomas, P. V. Brentano, R. M. Lieder, H. M. Jäger, H. Kämmerling, M. Berst, D. Gutknecht, and R. Henck, Nucl. Instrum. Methods Phys. Res. A **369**, 135 (1996).

[61] A. Såmark-Roth, D. M. Cox, J. Eberth, P. Golubev, D. Rudolph, L. G. Sarmiento, G. Tocabens, M. Ginsz, B. Pirard, and P. Quirin, Eur. Phys. J. A **56**, 141 (2020).

[62] U. Forsberg, Element 115, Ph.D. thesis, Lund University, 2016.

[63] U. Forsberg, D. Rudolph, P. Golubev, L. G. Sarmiento, A. Yakushev, L.-L. Andersson *et al.*, EPJ Web Conf. **66**, 02036 (2014).

[64] D. Rudolph, U. Forsberg, P. Golubev, L. G. Sarmiento, A. Yakushev, L.-L. Andersson *et al.*, Acta Phys. Pol. B **45**, 263 (2014).

[65] Ch. Lorenz, Quantum-state selective nuclear decay spectroscopy, Ph.D. thesis, Lund University, 2018.

[66] NNDC Evaluated Nuclear Structure Data File (ENSDF) Search and Retrieval, http://www.nndc.bnl.gov/ensdf/ (2016).

[67] G. Pausch, W. Bohne, and D. Hilscher, Nucl. Instrum. Methods Phys. Res. A **337**, 573 (1994).

[68] T. Kibédi, M. B. Trzhaskovskaya, M. Gupta, and A. E. Stuchberry, At. Data Nucl. Data Tables **98**, 313 (2012).

[69] C. Qi, F. R. Xu, R. J. Liotta, R. Wyss, M. Y. Zhang, C. Asawatangtrakuldee, and D. Hu, Phys. Rev. C **80**, 044326 (2009).
[70] J. L. Egido and A. Jungclaus, Phys. Rev. Lett. **126**, 192501 (2021).
[71] R. M. Clark and D. Rudolph, Phys. Rev. C **97**, 024333 (2018).
[72] T. Kibédi, T. W. Burrows, M. B. Trzhaskovskaya, P. M. Davidson, and C. W. Nestor, Jr., Nucl. Instrum. Methods Phys. Res. A **589**, 202 (2008).
[73] J. T. H. Dowie, T. Kibédi, T. K. Eriksen, and A. E. Stuchberry, At. Data Nucl. Data Tables **131**, 101283 (2020).
[74] T. Kibédi (private communication).
[75] J. F. Berger, M. Girod, and D. Gogny, Nucl. Phys. A **428**, 23 (1984).
[76] A. Baran, M. Kowal, P.-G. Reinhard, L. M. Robledo, A. Staszczak, and M. Warda, Nucl. Phys. A **944**, 442 (2015).
[77] F. P. Heßberger, Eur. Phys. J. A **53**, 75 (2017).
[78] J. Khuyagbaatar, Nucl. Phys. A **1002**, 121958 (2020).
[79] R. Smolańczuk, J. Skalski, and A. Sobiczewski, Phys. Rev. C **52**, 1871 (1995).
[80] R. Smolańczuk, Phys. Rev. C **56**, 812 (1997).
[81] P. Möller, A. J. Sierk, T. Ichikawa, A. Iwamoto, R. Bengtsson, H. Uhrenholt, and S. Åberg, Phys. Rev. C **79**, 064304 (2009).
[82] M. Albertsson, B. G. Carlsson, T. Døssing, P. Möller, J. Randrup, and S. Åberg, Eur. Phys. J. A **56**, 46 (2020).
[83] P. Möller and J. R. Nix, J. Phys. G: Nucl. Part. Phys. **20**, 1681 (1994).
[84] M. Albertsson, B. G. Carlsson, T. Døssing, P. Möller, J. Randrup, and S. Åberg, Phys. Lett. B **803**, 135276 (2020).
[85] W. Brodziński, P. Jachimowicz, M. Kowal, and J. Skalski, JPS Conf. Proc. **6**, 020054 (2015).
[86] A. Staszczak, A. Baran, and W. Nazarewicz, Phys. Rev. C **87**, 024320 (2013).
[87] J. L. Egido, J. Lessing, V. Martin, and L. M. Robledo, Nucl. Phys. A **594**, 70 (1995).
[88] M. Warda and J. L. Egido, Phys. Rev. C **86**, 014322 (2012).
[89] E. Garrote, J. L. Egido, and L. M. Robledo, Phys. Lett. B **410**, 86 (1997).